ISABE-2011-1220

STUDY OF NEAR-STALL FLOW BEHAVIOR IN A MODERN TRANSONIC FAN WITH COMPOSITE SWEEP

Chunill HAH[1], Hyoun-Woo Shin[2]

[1]NASA Glenn Research Center,
MS 5-11, Cleveland, Ohio 44135
[2]Aero Technology Lab.
GE Aviation, Cincinnati, Ohio, 45215

ABSTRACT

Detailed flow behavior in a modern transonic fan with a composite sweep is investigated in this paper. Both unsteady Reynolds-averaged Navier-Stokes (URANS) and Large Eddy Simulation (LES) methods are applied to investigate the flow field over a wide operating range. The calculated flow fields are compared with the data from an array of high-frequency response pressure transducers embedded in the fan casing. The current study shows that a relatively fine computational grid is required to resolve the flow field adequately and to calculate the pressure rise across the fan correctly. The calculated flow field shows detailed flow structure near the fan rotor tip region. Due to the introduction of composite sweep toward the rotor tip, the flow structure at the rotor tip is much more stable compared to that of the conventional blade design. The passage shock stays very close to the leading edge at the rotor tip even at the throttle limit. On the other hand, the passage shock becomes stronger and detaches earlier from the blade passage at the radius where the blade sweep is in the opposite direction. The interaction between the tip clearance vortex and the passage shock becomes intense as the fan operates toward the stall limit, and tip clearance vortex breakdown occurs at near-stall operation. URANS calculates the time-averaged flow field fairly well. Details of measured RMS static pressure are not calculated with sufficient accuracy with URANS. On the other hand, LES calculates details of the measured unsteady flow features in the current transonic fan with composite sweep fairly well and reveals the flow mechanism behind the measured unsteady flow field.

INTRODUCTION

Transonic fans with various blade sweeps have been developed as crucial components of modern ultra-high bypass engine concepts. The development aims to achieve higher thrust and higher aerodynamic efficiency with the potential for reducing noise and emissions. The transonic fan in this study with a composite blade sweep has been developed by the General Electric Company and tested at the NASA Glenn Research Center. The 0.559 m (22 inch) diameter model was supported and driven by the Universal Propulsion Simulator (UPS), which was designed for evaluating configurations of high bypass ratio ducted fan engines. The averaged tip clearance is 0.5% of the blade height and the tested fan model has 20 blades. The aerodynamic test was conducted at the 9x15-Foot Low Speed Wind Tunnel, which is located at the NASA Glenn Research Center in Cleveland, Ohio. The cross section of the tested fan is shown in Fig. 1.

The flow field near the fan casing is very complex. Dominant features of the compressor endwall flow include the tip clearance flow; interactions among the tip clearance flow, the passage shock, and the endwall boundary layers; and accumulation of low momentum fluid due to radial migration.

Tip clearance flow in fans and compressors has been widely studied (for example Hah [1986], Copenhaver et al. [1996], Storor and Cumpsty [1991], Suder and Celestina [1994], Van Zante et al. [2000]). Tip clearance flow arises from the pressure difference between the pressure and the suction side in the tip gap area. Flow through the tip gap interacts with the incoming passage flow near the suction side of the blade as it leaves the blade tip section, forming

the tip clearance vortex. The vortex core is formed by fluid originating from the leading edge of the blade. Fluid flowing over the remainder of the blade rolls around this core vortex and adds swirl intensity. Some tip clearance flow originating near the casing travels over to the tip gap of the adjacent blade, resulting in so called double leakage flow (Smith [1993]). Near the stall condition, the pressure difference across the blade tip section increases and the interaction between the tip clearance flow and the passage flow becomes stronger. This causes more mixing losses and an increase in aerodynamic blockage near the casing. In transonic rotors, strong interaction between the tip clearance vortex and the blade passage shock is expected when the rotor operates at near-stall condition.

Various recent studies (for example, Schlechtriem and Lostzerich [1997], Hoffmann and Ballmann [2003], and Yamada et al. [2003]) have proposed tip vortex breakdown as a possible cause of stall inception in transonic compressor rotors. Vortex breakdown is defined as a phenomenon in which an abrupt change in the vortex core structure occurs. In transonic compressors, it is argued that shock/tip-vortex interaction can cause such vortex breakdown. Blade sweep has been extensively investigated to control flow structures, especially near the tip (for example, Wadia et al. [1993] and Breugelmans et al. [1984]). Simple forward sweep is commonly introduced to extend stall margin in many transonic fan designs. A composite blade sweep is applied to increase aerodynamic efficiency as well as stall margin by controlling flow structures in modern fan designs.

The flow field becomes transient as the fan operates toward the stall limit. Interaction between the tip clearance flow and the passage shock becomes unsteady, and the tip clearance flow becomes oscillatory as a consequence. Detailed measurement of unsteady velocity components inside the tip clearance is highly desirable to understand detailed flow structures at this critical operating condition as well as to validate any unsteady flow simulations. Although great advances have been made in flow measurement technology in turbomachinery over the last decade, it has not been possible to measure the unsteady velocity field near the rotor tip area. Most useful unsteady flow measurements have been obtained through casing-mounted pressure transducers. To understand end wall flow structures adequately, the unsteady velocity field below the casing should be measured accurately. Most previous analytical studies of tip clearance flow have been based on steady flow assumptions. Although tip clearance flow is generated by the pressure difference across the blade tip, the pressure field is transient when the rotor operates near stall. Also, the stall inception process is transient. Therefore, unsteady characteristics of tip clearance flow and its interaction with the passage shock should be properly investigated.

In the present study, the effects of loading on tip clearance vortices, passage shocks and their interaction in a transonic fan with a composite blade sweep are investigated. Both URANS and LES methods are applied to simulate fan flow fields at various operating conditions. The calculated flow fields are analyzed and compared with the measured data from conventional pressure probes and high-frequency-response pressure sensors embedded on the casing.

TEST FACILITY AND UNSTEADY DYNAMIC PRESSURE MEASUREMENTS

The 20-blade fan model was tested in the 9x15-Foot Low Speed Wind Tunnel, which is an anechoic wind tunnel facility located at the NASA Glenn Research Center, Cleveland, Ohio. The facility is operated as an open loop, continuous flow wind tunnel at atmospheric pressure. Low free stream turbulence and distortion levels at the fan inlet make the test facility ideal for acoustic testing of propulsion systems.

Figure 2 shows a removable pressure block installed on the fan casing. A total of 21 ultra-miniature high-frequency pressure transducers are installed. The frequency response of the transducers is 70 KHz. The unsteady data from these transducers and pneumatically-averaged pressure data are used to study flow structures near the fan rotor tip. Further details of the flow measurements and data processing are given by Shin et al. [2008].

NUMERICAL PROCEDURE

Both URANS and LES methods are applied in the present study. URANS was first applied to obtain the fan speed line and to compare the overall flow structures at various operating conditions with the measured data. The LES procedure was applied primarily to capture transient characteristics of the tip clearance vortex more realistically at near-stall operation. A standard two-equation turbulence model was used for the URANS. A Smagorinsky-type eddy-viscosity model was used for the subgrid stress tensor, and the standard dynamic model by Germano et al. [1991] was applied for the LES.

In the current study, the governing equations are solved with a pressure-based implicit method using a fully conservative control volume approach. A third-order accurate interpolation scheme is used for the discretization of convection terms and central differencing is used for the diffusion terms. The method is of second-order accuracy with smoothly varying grids. For the time-dependent terms, an implicit second-order scheme is used and a number of sub-iterations are performed at each time step. Details of the numerical method and applications to transonic flows are given by Hah and Wennerstrom [1991].

An initial grid with about 1,000,000 nodes was first applied for the URANS simulation. However, the calculated pressure field did not agree well with the measurements. The URANS grid was refined to 2,030,400 nodes for better agreement with measurements. For the LES simulation, the grid was further refined to 9,356,688 nodes, with 198 nodes in the blade-to-blade direction, 88 nodes in the spanwise direction, and 537 nodes in the streamwise direction. The inflow boundary was located 2 average blade heights upstream of the rotor leading edge and the outflow boundary was located three blade heights from the trailing edge. The rotor tip clearance geometry is accurately represented by 28 nodes in the blade-to-blade direction, 20 nodes in the

spanwise direction, and 140 nodes in the streamwise direction. I-grid topology is used to reduce grid skewness and a single-block grid is used. All the computations were performed with NASA's Columbia supercomputer system, which allows parallel computation with up to 512 processors.

Standard boundary conditions for an isolated rotor were applied at the boundaries of the computational domain. Circumferentially averaged static pressure at the casing was specified to control the mass flow rate. Non-reflecting boundary conditions were applied at the inlet and the exit boundaries.

OVERALL FLOW STRUCTURE

Measured and calculated pressure-rise characteristics of the fan at 104% of the design rotor speed are shown in Fig. 3. The LES simulation was performed at near-stall condition where the interactions between the tip clearance vortex and passage shock intensify. Averaged flow properties were obtained by averaging 10,000 instantaneous solutions for both URANS and LES. URANS calculates the overall fan performance fairly well although the calculated the pressure rise is about 3% higher than the measured value. At the near-stall condition, the calculated pressure rise from LES is slightly lower than that from URANS and matches the measured value better. In the following sections, flow structures near the fan tip at three operating conditions are analyzed with both measured data and calculations from URANS and LES.

TIP VORTEX AND SHOCK STRUCTURE AT CHOKE CONDITION

The measured ensemble-averaged static pressure distribution and corresponding RMS static pressure at the casing at choke condition (point 1 in Fig. 3) are shown in Fig. 4. A small island of raised pressure adjacent to the concave side of the blade is marked as "X" in Fig. 4. Both the leading edge vortex and another tip clearance vortex from the mid-chord are also marked in Fig. 4.

Calculated endwall static pressure and RMS static pressure are given in Fig. 5. The calculated static pressure and RMS pressure distributions agree with the measured fields very well. The raised pressure region near the pressure side of the blade and overall shock structures are calculated very well with URANS. The calculated RMS static pressure is higher at the passage shock while the value at the leading edge oblique shock is lower than the measured value. The calculated flow field shows that the second tip clearance vortex initiates where the passage shock meets the suction side of the blade. After the passage shock, the static pressure increases suddenly on the pressure side while the pressure near the suction side remains about the same. This results in a large difference in pressure across the blade at this location, creating the second tip clearance vortex which was also shown in the measurement. Both calculated and measured RMS pressure show that this second vortex is much stronger than the tip clearance vortex originating near the leading at this operating condition.

Figure 6 compares static pressure rise across the fan between measurements and time-averaged URANS. The leading edge and the trailing edge of the blade are located at non-dimensional axial coordinates of 0.317 and 0.926. As reported by Shin et al. [2008], pressure rise from the time-averaged high-frequency probe matches fairly well with the steady pressure probe. However, it seems that changes in the pressure filed due to complex flow structures in the tip region are picked up better by the high-frequency probe. The overall pressure rise from URANS follows measured values from the high-frequency probe. However, URANS calculates higher pressure before the passage shock and lower values after the passage shock. It is believed that precise calculation of static pressure rise across transonic fans is often difficult. The pressure rise is rather sensitive to the viscous boundary layer growth. In addition, the true casing contour and exact tip clearance geometry might be required for the precise calculation of the pressure rise.

Overall, URANS calculates the complex flow structure at the choke condition fairly well and the calculated flow field explains the flow mechanism behind the measured flow field.

TIP VORTEX AND SHOCK STRUCTURE AT NEAR PEAK EFFICIENCY CONDITION

Figure 7 shows measured ensemble-averaged static pressure and corresponding RMS static pressure at the near-peak-efficiency condition (operating point 2 in Fig. 3). Calculated distributions are shown in Fig. 8. Both the measured and calculated distributions show that the passage shock is located near the leading edge. Consequently, a strong tip clearance vortex is formed near the leading edge. Calculated structures of the passage shock and tip clearance vortex agree very well with the measured structures.

Figure 9 shows the calculated static pressure distribution at 50% span. At this location the passage shock is already detached from the leading edge although the passage shock stays very close to the leading edge at the fan tip as shown in Figure 8. The three dimensional shock structures shown in Figures 8 and 9 are due to introduction of composite sweep of the fan blade. Both the measured and calculated RMS pressures show strong oscillation of the passage shock. On the other hand, the tip clearance vortex shows relatively small RMS pressure, which indicates that the tip clearance vortex is not oscillating at this operating condition. Both the measurements and the calculations show high RMS levels in the region where the passage shock interacts with the suction surface of the blade. Due to the sudden increase of the streamwise pressure gradient, flow separation is likely in this area. Neither the measured data nor the URANS results with the current computational grid show clear flow separation in this area.

Figure 10 compares measured and URANS-calculated static pressure rise across the fan. The agreement between the measurements and the calculation is considered to be reasonable.

TIP VORTEX AND SHOCK STRUCTURE AT NEAR STALL CONDITION

Figure 11 shows the measured ensemble-averaged static pressure distribution and the corresponding RMS static pressure at the casing at the near-stall condition (point 3 in Fig. 3). Measured static pressure in Fig. 11 shows a region of higher pressure near the pressure-side of the blade close to the leading edge.

Static pressure and RMS static pressure distributions from the URANS simulation are given in Fig. 12. The overall static pressure distribution from URANS agrees fairly well with the measurements. The region of high pressure near the leading edge (marked as "X" in Fig. 11) is not clearly calculated by URANS.

The measured RMS static pressure distribution (Fig. 11) shows several areas of high periodic unsteadiness. Zone "A" is the signature of the tip clearance vortex that originates near the leading edge. Zone "B" is due to the oscillation of the bow shock. Zone "C1" has higher RMS values than zone "A". High RMS values in Zone "C1" are due to the interaction between the tip clearance vortex and the shock. The high value of RMS in zone "C1" indicates that the tip clearance vortex/shock interaction is an inherently unsteady phenomenon as suggested by Thomer et al. [2002]. The zone marked "C2" is not related to the tip clearance vortex. As suggested by Shin et al. [2008], this high RMS area could be due to the roll-up of the casing boundary layer after the bow shock. Zone "E" is due the tip clearance vortex originating from the mid-chord of the blade tip. Zone "D" is not located on the path of the tip clearance vortex from the leading edge.

Figure 13 shows instantaneous casing pressure distributions at three equally spaced time steps during one cycle of tip vortex oscillation from the LES simulation. Averaged static pressure and RMS static pressure distributions are given in Fig. 14. Changes in the pressure field in Fig. 13 indicate that the tip clearance vortex core oscillates substantially as it interacts with the passage shock, and tip clearance vortex breakdown occurs as it goes through the passage shock at this operating condition. The averaged static pressure field matches the measured static pressure filed better than that from URANS shown in Fig. 12.

RMS static pressure and averaged velocity vectors at the blade tip from LES are given in Fig. 15. The calculated RMS static pressure distribution agrees very well with the measurement. All the measured unsteady flow features near the casing are well calculated by LES. The high RMS region "C2" is not on the direct path of tip clearance vortex and flow traces show that this high RMS region is due to the roll up of the casing boundary layer as indicated by Shin et al [2008]. The high RMS static pressure area "D" is due to interaction between the tip clearance flow from the mid-chord and the tip leakage flow from the trailing edge area.

The calculated average velocity field shows that the flow at the leading edge spills over into the adjacent passage. However, flow at the trailing edge is not reversed. The fan operates in a stable mode at this operating condition even though the flow at the leading edge spills into the next passage, which confirms the stall criteria suggested by Vo et al. [2005].

Measured RMS static pressure shows the complex nature of the unsteady pressure field at the near-stall operating condition. Static pressure rise across the fan from the measurements, URANS and LES are compared in Fig. 16. Averaged static pressure rise from the high-frequency-response pressure transducers seems to capture the influence of complex flow structures better than the conventional probe. The pressure rises calculated from URANS and LES show large variations near the leading edge and match the overall trend from the high-frequency transducers fairly well.

The stall inception mechanism is directly related to the unsteady characteristics of the tip clearance flow. Therefore any effective flow control mechanism must account for unsteady aspects of the flow field. The comparisons with the measured data show that URANS might not be an effective tool to study detailed unsteady flow fields in transonic fans.

CONCLUDING REMARKS

Changes in flow structure near the end wall in a modern transonic fan with composite blade sweep were studied with both URANS and LES. Calculated flow fields were compared with the measured data from high-frequency pressure transducers. URANS calculates the averaged flow field very well. However, details of the unsteady flow characteristics due to the flow interaction in the tip region are not calculated accurately with URANS. LES captures details of the measured unsteady flow features very well and explains underlying flow mechanism of the measured unsteady flow field. Accurate and reliable unsteady flow calculation, including flow separation, is very desirable for developing advanced transonic fans and flow control devices for improved aerodynamic efficiency and wider operating ranges.

REFERENCES

Breugelmans, F.A.E., Carels Y., and Demuth, M., 1984, "Influence of Dihedral on the Secondary Flow in a Two-Dimensional Compressor Cascade," ASME Journal of Engineering for Gas Turbines and Power, Vol. 106, pp. 578-584.

Copenhaver, W. W., Mayhew, E. R., Hah, C., and Wadia, A. R., 1996, "The Effects of Tip Clearance on a Swept Transonic Compressor Rotor,'' ASME Journal of Turbomachinery, Vol. 118, pp. 230-239.

Germano, M., Piomelli, U., Moin, P., and Cabot, W. H., 1991, "A Dynamic Subgrid-Scale Eddy-Viscosity Model," Journal of Fluid Mechanics, Vol. A3, pp. 170-176.

Hah, C., 1986, "A Numerical Modeling of Endwall and Tip-Clearance Flow of an Isolated Compressor," ASME Journal of Engineering for Gas Turbines and Power, Vol. 108, No. 1, pp. 15-21.

Hah, C. and Wennerstrom, A. J., 1991, "Three-Dimensional Flow Fields Inside a Transonic Compressor with Swept

Blades," ASME Journal of Turbomachinery, Vol. 113, No. 1, pp. 241-251.
Hoffman, W. H. and Ballman, J., 2003, "Some Aspects of Tip Vortex Behavior in a Transonic Turbocompressor," ISABE Paper 2003-1223.
Schlechtriem, S. and Loetzerich, M., 1997, "Breakdown of Tip Leakage Vortices in Compressors at Flow Conditions Close to Stall,'' ASME Paper 97-GT-41.
Shin, H., Solomon, W., and Wadia, A., 2008, "Transonic Fan Tip-Flow Features Revealed by High Frequency Response Over-Tip Pressure Measurements," ASME Paper GT2008-50279.
Smith L. H. Jr., 1993, Private communication.
Suder, K. L., and Celestina, M. L., 1994, "Experimental and Computational Investigation of the Tip Clearance Flow in a Transonic Axial Compressor Rotor,'' NASA TM-106711.
Storer, J. A. and Cumpsty, N. A., 1991,"Tip Leakage Flow in Axial Compressors," ASME Journal of Turbomachinery, Vol. 113, pp. 252-259.
Thomer, O., Klass, M., Schroeder, W., and Krause, E., 2002, "Interaction between Longitudinal Vortices and Normal and Oblique Shocks," Proceedings of Fifth World Congress on Computational Mechanics.
Van Zante, D. E., Strazisar, A. J., Wood, J. R., Hathaway, M. D., Okiishi, T. H., 2000, "Recommendations for Achieving Accurate Numerical Simulation of the Tip Clearance Flows in Transonic Compressor Rotors,'' ASME Journal of Turbomachinery, Vol. 122, pp. 733-742.
Wadia, A. R., Szuch, P. N., and Crall, D., 1997, "Inner Workings of Aerodynamic Sweep," ASME Paper 97GT-401.
Yamada, K, Furukawa, M., Inoue, M., and Funazaki, K., 2003, "Numerical Analysis of Tip Leakage Flow Field in a Transonic Axial Compressor Rotor," IGTC Paper 2003-095.
Vo, H D., Tan, C. S., and Greitzer, E. M., 2005, "Criteria for Spike Initiated Rotating Stall," ASME Paper GT2005-68374.

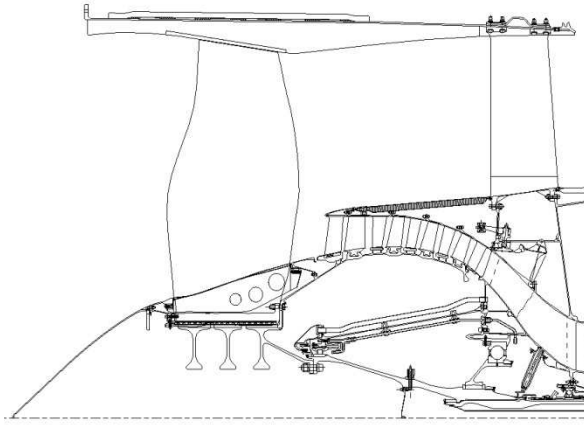

Figure 1: Cross section of test fan.

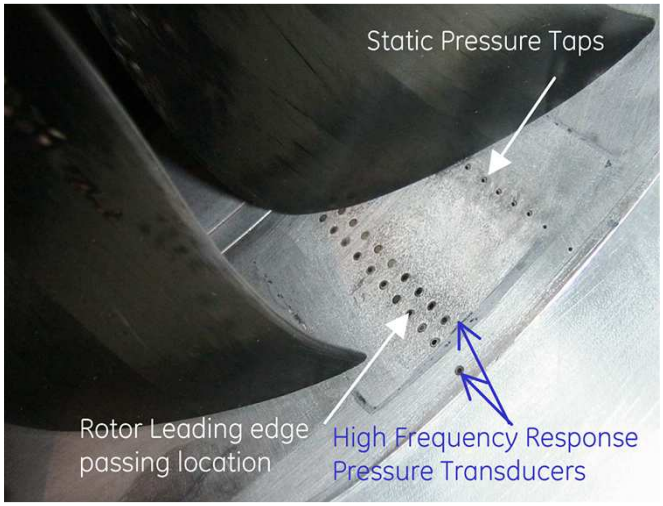

Figure 2: View of casing with pressure block..

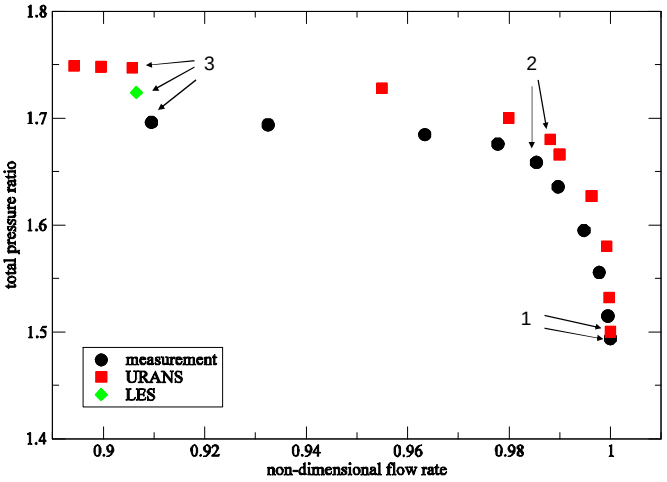

Figure 3: Three operating points for comparison.

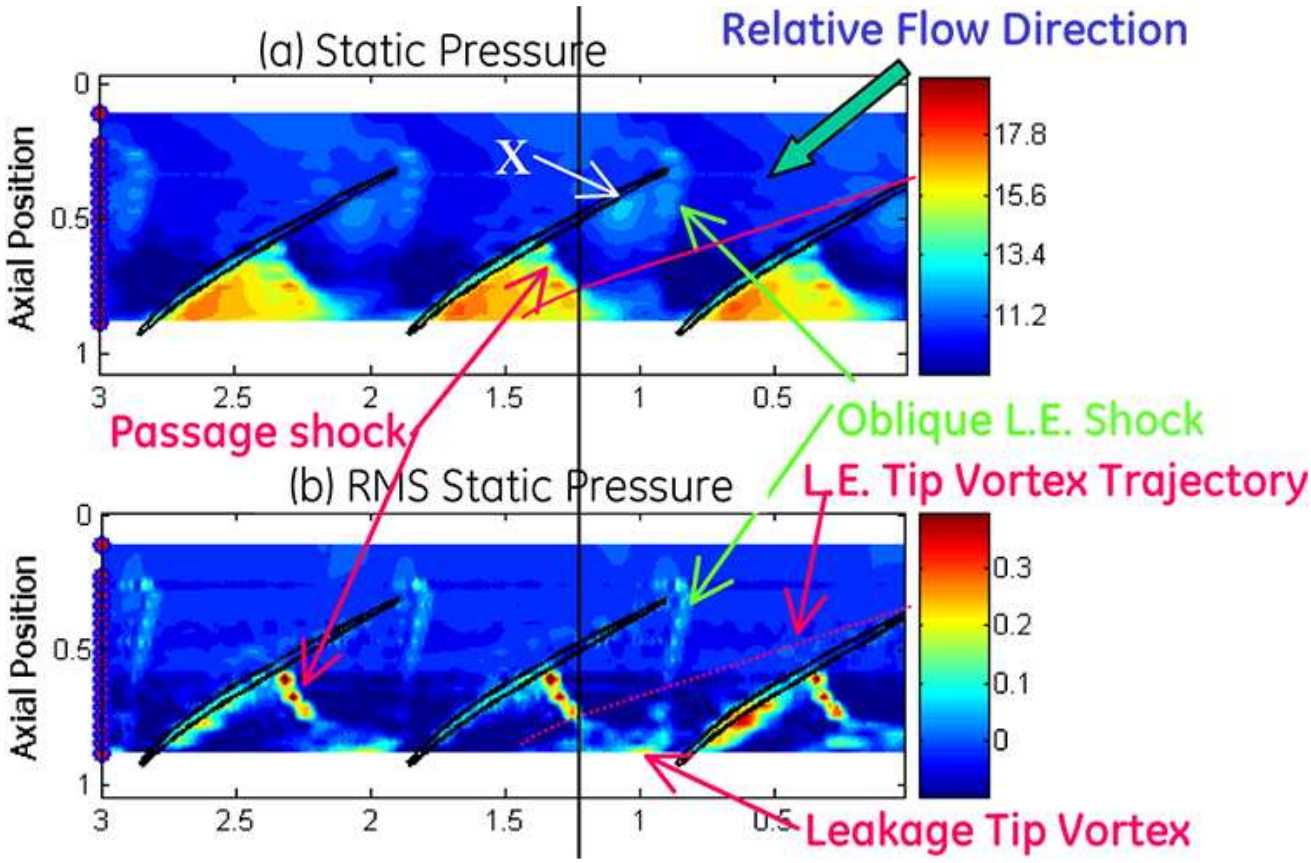

Figure 4: Measured static pressure and RMS static pressure at choke condition (Point 1 in Fig.3).

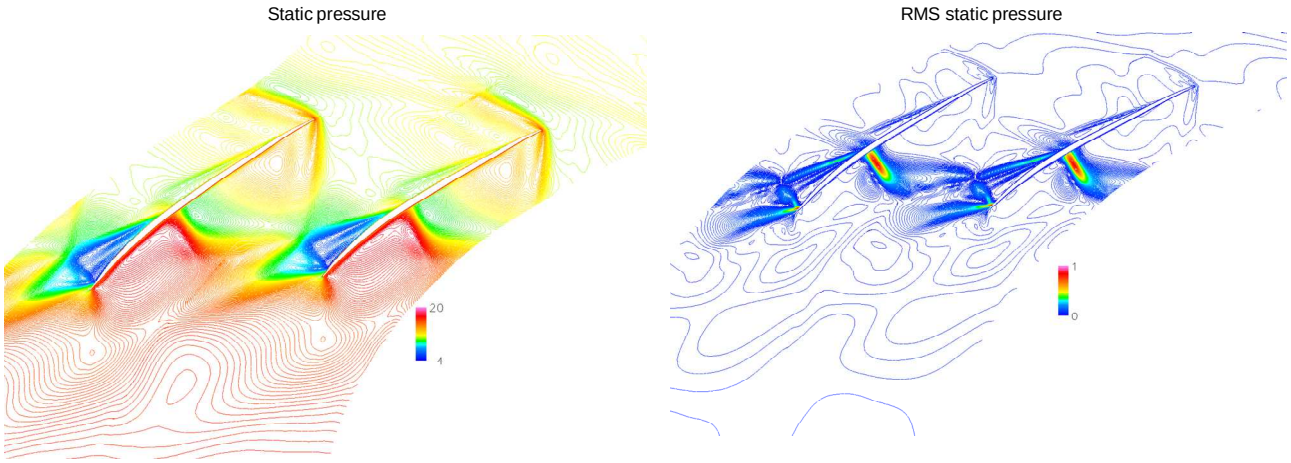

Figure 5: Calculated static pressure and RMS static pressure at choke condition (Point 1 in Fig.3), URANS.

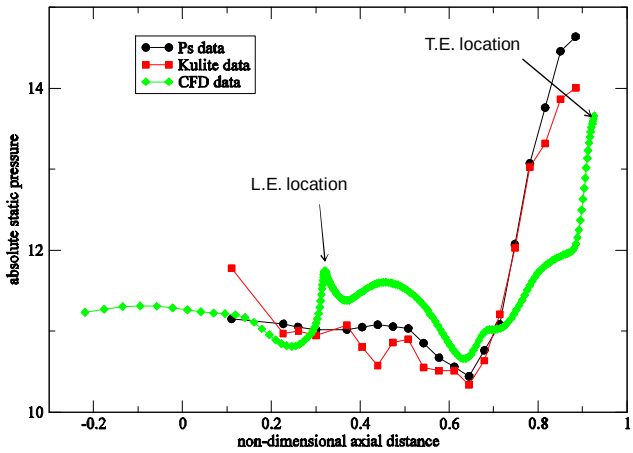

Figure 6: Comparison of steady static pressure rise at choke condition (Point 1 in Fig. 3).

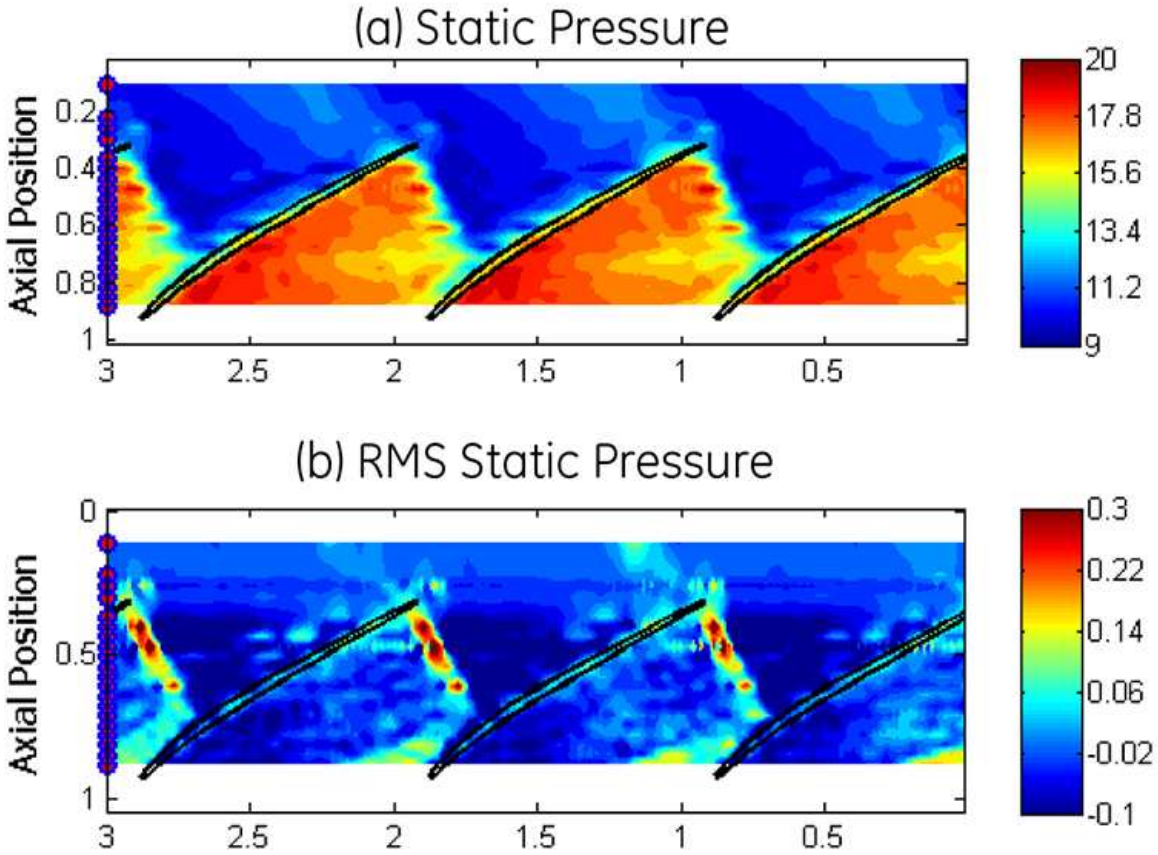

Figure 7: Measured static pressure and RMS static pressure at peak efficiency condition (Point 2 in Fig.3).

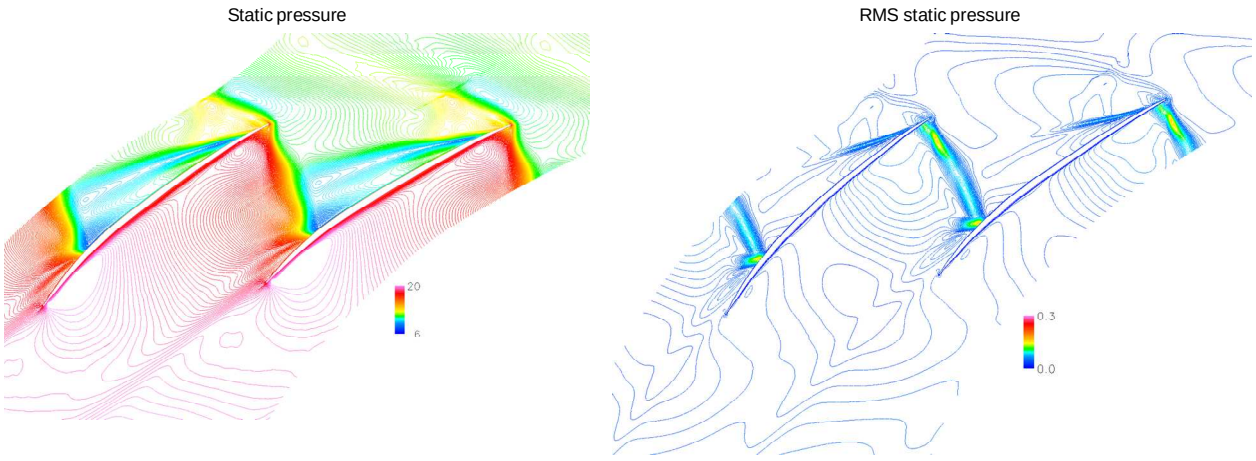

Figure 8: Calculated static pressure and RMS static pressure at peak efficiency condition (Point 2 in Fig.3), URANS.

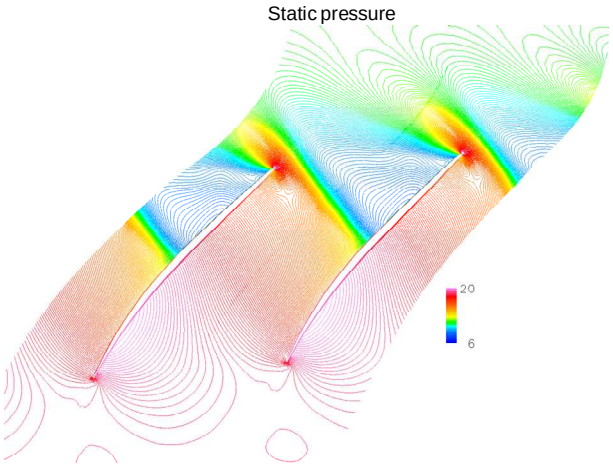

Figure 9: Calculated static pressure at 50% span at peak efficiency point.

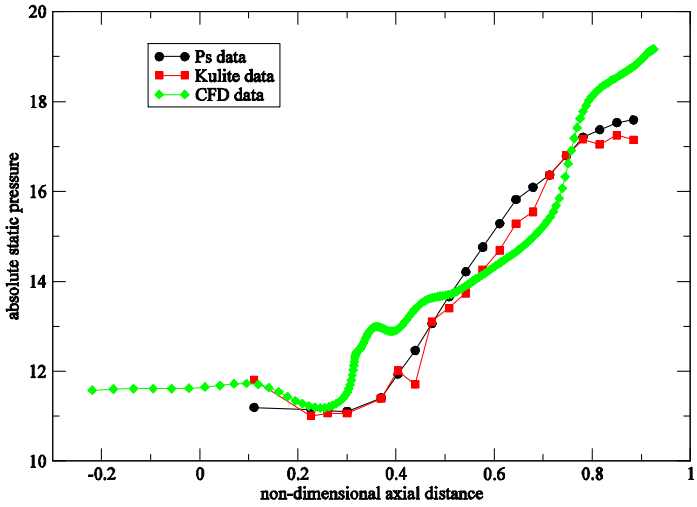

Figure 10: Comparison of steady static pressure rise at peak efficiency condition (Point 2 in Fig. 3).

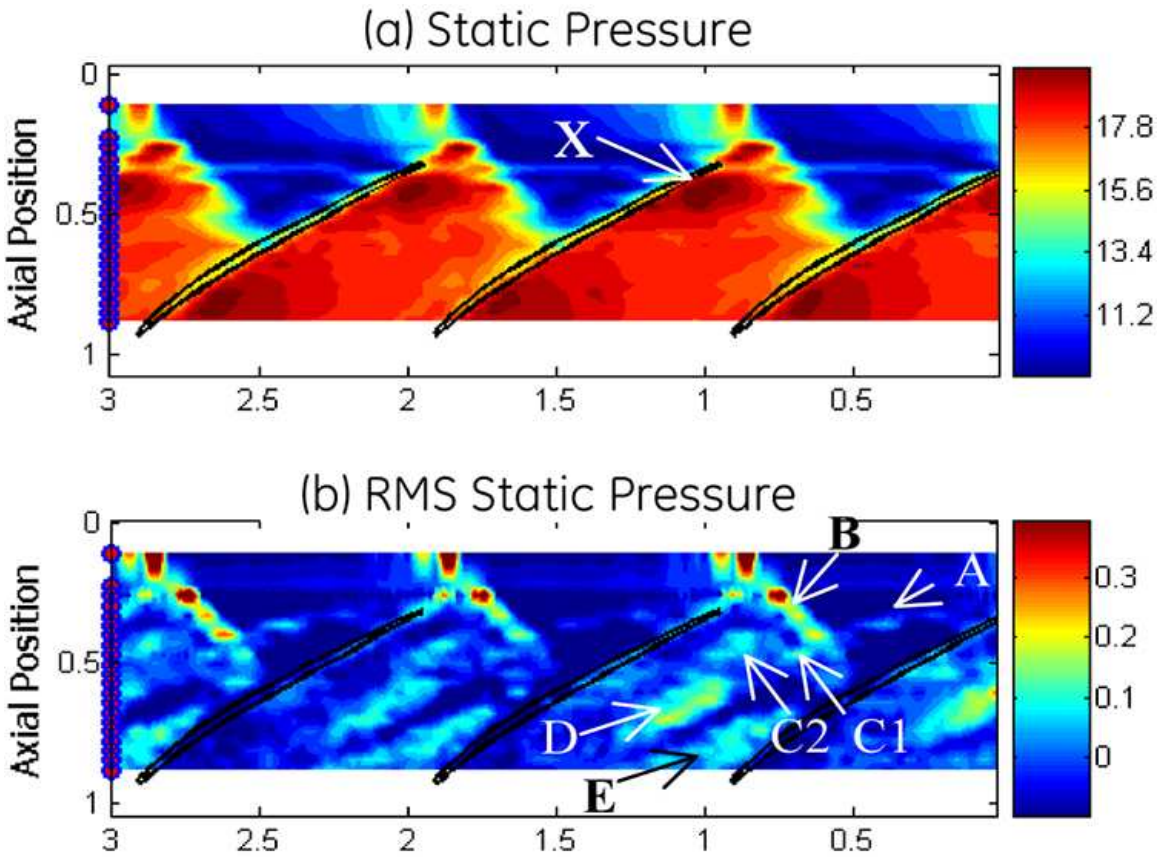

Figure 11: Measured static pressure and RMS static pressure at near-stall condition (Point 3 in Fig.3).

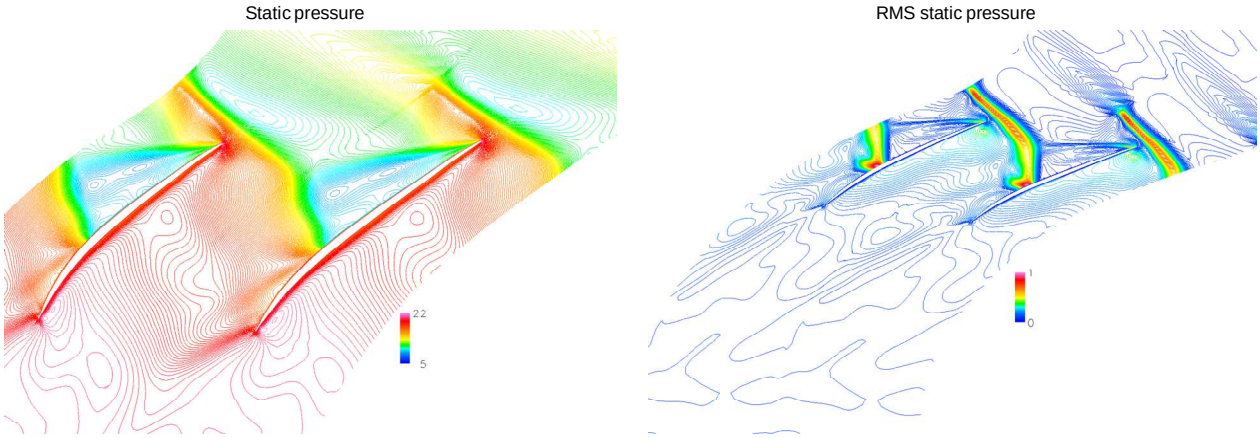

Figure 12: Calculated static pressure and RMS static pressure at near stall condition (Point 3 in Fig.3), URANS.

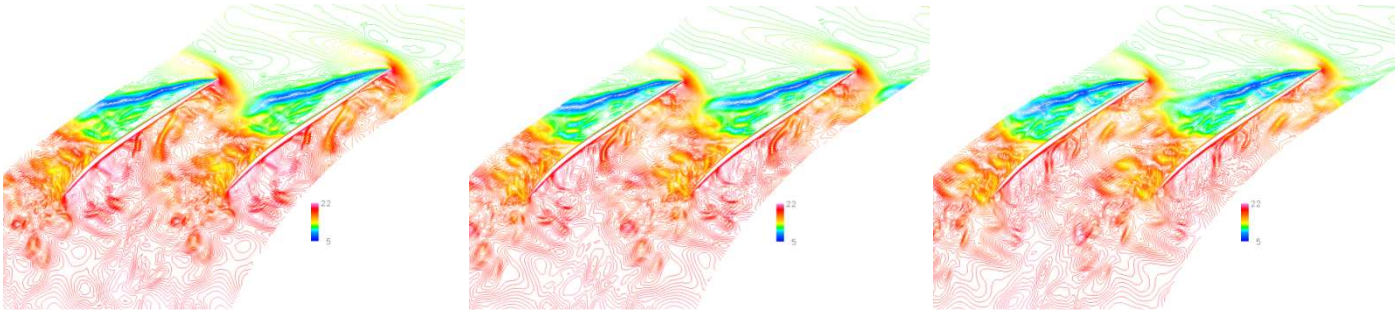

Time 1 Time 2 Time 3

Figure 13: Changes in static pressure distribution at the fan tip at near stall operation (Point 3 in Fig.3), LES.

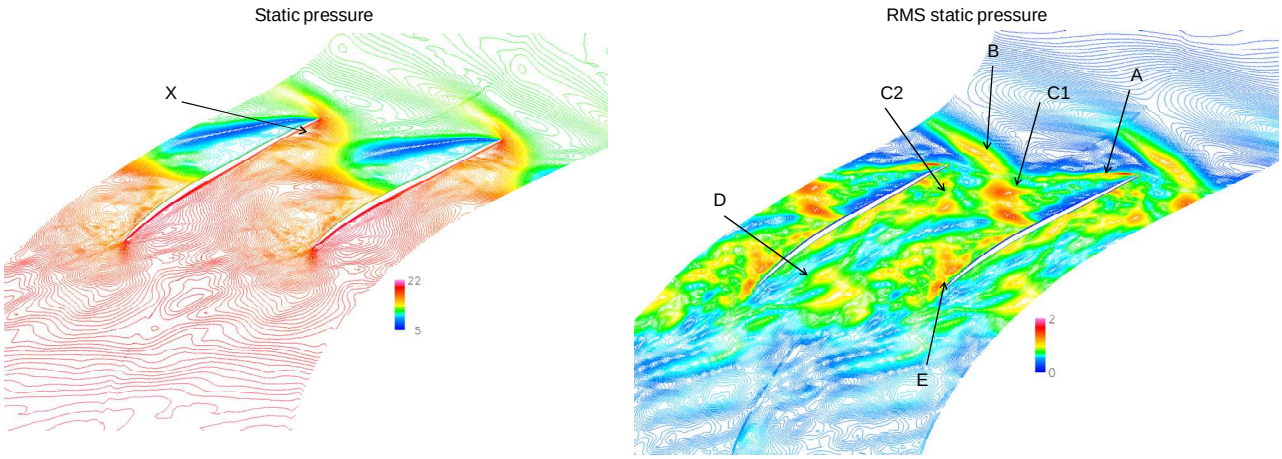

Figure14: Calculated static pressure and RMS static pressure at near stall condition (Point 3 in Fig.3), LES.

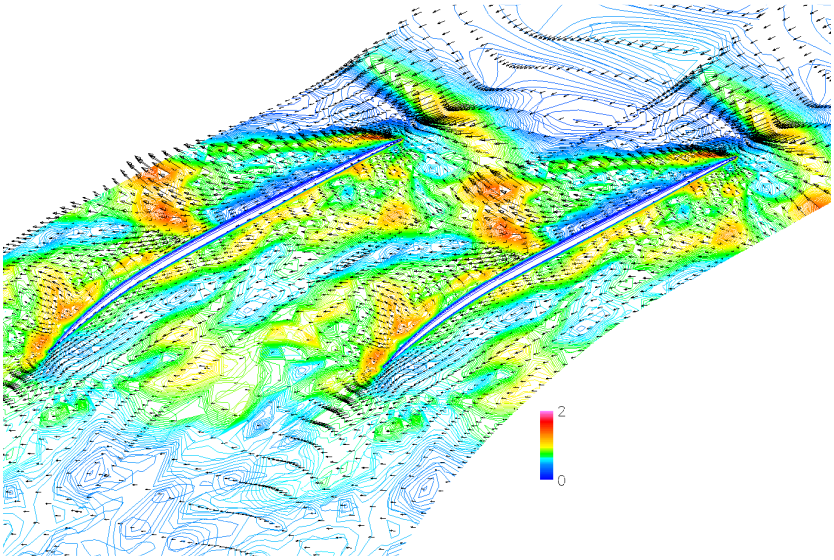

Figure 15: RMS static pressure distribution and averaged velocity vectors at fan tip, near stall (Point3 in Fig. 3), LES.

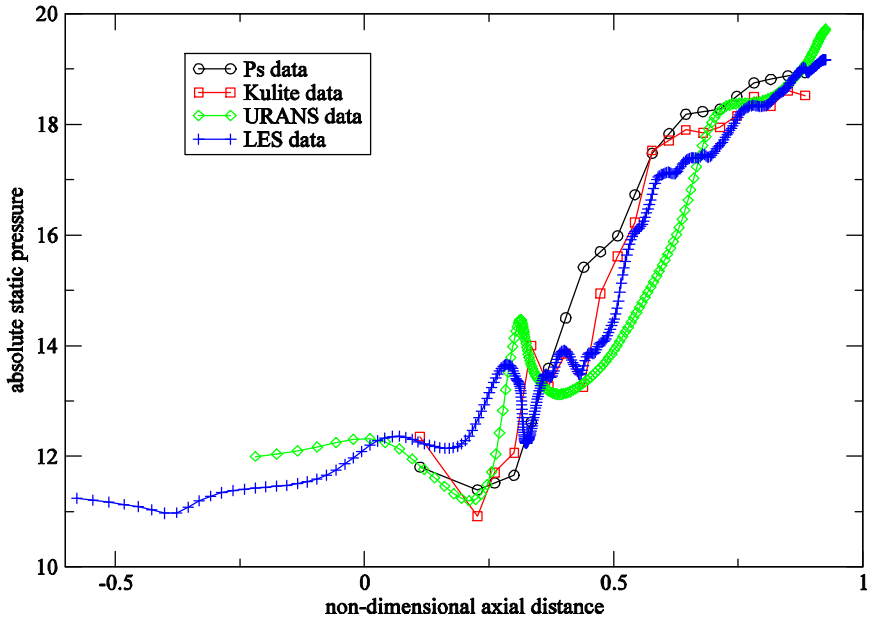

Figure 16: Comparison of steady static pressure rise at near stall condition (Point 3 in Fig. 3).